Analyzing past and future droughts that induce clay shrinkage in France using an index based on water budget simulation for trees

Sophie Barthelemy[1,2,3], Bertrand Bonan[1], Miquel Tomas-Burguera[1,a], Gilles Grandjean[2], Séverine Bernardie[2], Jean-Philippe Naulin[3], Patrick le Moigne[1], Aaron Boone[1], and Jean-Christophe Calvet[1]

[1]CNRM, Université de Toulouse, Météo-France, CNRS, Toulouse, France

[2]Bureau de Recherches Géologiques et Minières (BRGM), Orléans, France

[3]Caisse Centrale de Réassurance (CCR), Dpt R&D Modeling Cat & Agriculture, Paris, France

[a]Now at University of the Balearic Islands, Palma, Balearic Islands, Spain, and Natural Hazards and Emergencies Observatory of the Balearic Islands, Inca, Balearic Islands, Spain

Correspondence to: Jean-Christophe Calvet (jean-christophe.calvet@meteo.fr)

Abstract. Clay shrinkage is the retraction of clayey soils under dry conditions, caused by the loss of adsorbed water molecules from clay minerals. This phenomenon called clay-shrinkage induced subsidence can cause permanent damage to buildings if the drying extends below the foundations. In France, soils with these characteristics are widespread, affecting 48 % of the mainland territory (MTES, 2021), resulting in damage amounting to 20.8 billion euros since 1989 (CCR, 2023b). The causes of clay shrinkage are not yet fully understood, particularly at large spatial scales that are critical for land management. In a previous study (Barthelemy et al., 2023), a drought index designed specifically for clay shrinkage was created. It is a yearly index called the year drought magnitude. This index measures the daily soil moisture anomaly over the course of a year, based on the Interactions between Soil, Biosphere, and Atmosphere (ISBA) land surface model of Météo-France. Its properties have been fine-tuned by comparing it to a sample of insurance data. As a continuation of this work, our aim is to analyze past and future soil moisture drought events that may cause subsidence by calculating yearly drought magnitudes for France. Prior to this, we refined the ISBA configuration by focusing solely on tree vegetation types. Historical and projected simulations were conducted with the main difference being the meteorological forcing provided to ISBA. The historical simulation covered the years 2000-2022 and used the SAFRAN atmospheric reanalysis, while the projected simulation covered the years 2006-2065 and used an ensemble of climate models under Representative Concentration Pathway (RCP) 4.5 and RCP 8.5. The historical simulation revealed significant soil moisture droughts in France in 2003, 2018, 2019, 2020, and 2022. In 2022, there were notably high index values throughout the country. The projected simulation indicated that drought conditions are expected to worsen in the future, particularly under RCP 8.5 compared to RCP 4.5. The scenarios diverged significantly after 2046, and both the north and south of the country were equally affected. Differences between historical and projected year drought magnitudes were observed: projections are more pessimistic on average and more optimistic regarding extreme events. This discrepancy can be explained either by differences in climate forcing or by differences in the vegetation response of the land surface scheme.

1 Introduction

Soil moisture refers to the water stored in the unsaturated zone of the soil. Despite representing only 0.05% of total freshwater (Gleick et al. 1993), this reservoir plays a crucial role in climate-determining physical processes by interacting with adjacent

35   land surface components. It is linked to the atmosphere in terms of both water and energy balance (Seneviratne et al., 2010). Water is exchanged through precipitation (positive fluxes) and evapotranspiration (negative fluxes). However, not all precipitation infiltrates into the soil. Some is intercepted by vegetation and evaporates before reaching the ground, while some runs off into surface reservoirs such as rivers and lakes. Evapotranspiration, which is the sum of bare soil evaporation, interception, and plant transpiration, requires a significant amount of energy to go from liquid to vapor phase and therefore

40   has a significant impact on the energy balance. Vegetation should not be overlooked as it contributes the most to total land evapotranspiration on the global scale (Seneviratne et al., 2010). After entering the soil, some water moves to groundwater reservoirs through gravity (drainage). The soil retains moisture through capillary forces exerted by its granular structure. The water-holding capacity of the soil and the intensity of the forces depend on the characteristics of the pore network and the texture of the soil. Additionally, soil moisture distribution and evolution are heterogeneous within the soil volume. This

45   distribution is influenced by local soil texture variations, as well as distance from the surface and the presence of vegetation roots.

In situ observations of soil moisture are scarce. Modeling soil moisture evolution over time is challenging due to the complexity of the system. Therefore, it is recommended to use land surface models (LSMs) instead of simpler alternatives (Berg and Sheffield, 2018). Soil moisture modeling is crucial for water resource management and weather forecasting because it affects

50   water and energy balances (Dirmeyer et al., 2021). Soil moisture can affect the carbon cycle, as seen in Europe during the summer of 2003 when vegetation suffered from extreme drought and became a carbon source (Ciais et al., 2005). Soil moisture variability can also impact human activities that depend on it. Episodes of low moisture, also known as agricultural droughts, can have catastrophic consequences for agriculture and forestry when they occur over extended periods of time (Moravec et al., 2021).

55   Dry soils can cause shrinkage due to soil particles losing their adsorbed water molecules. This volume change is specific to clay minerals such as smectite, vermiculite, montmorillonite, which are formed by weathering and found in surface deposits that are inherently heterogeneous. Soil shrinkage can cause irreversible damage to buildings when differencial displacements occur between dry clay soil and the soil beneath the foundation, resulting in cracks in walls as evidence of deformation. This phenomenon is known as clay shrinkage induced subsidence. It is a global issue, as described by Barthelemy et al. (2023), and

60   has been extensively studied (Meisina et al., 2006; Vincent et al., 2009; Soubeyroux et al., 2011; Hawkins, 2013; Gourdier and Plat, 2018; Mostafiz et al., 2021; Tzampoglou et al., 2022). In France, this phenomenon affects 48% of the territory to a moderate or strong degree (MTES, 2021). The "CatNat" (NatCat) scheme is a system under which the French state compensates for damages caused by natural disasters, including droughts that cause clay shrinkage. According to CCR

(2023b), this hazard costed 2.9 billion euros in compensations for 2022, while a total of 20.8 billion euros has been spent since 1989. The cost of damages has reached an unprecedented level since 2017.

Increasing atmospheric CO_2 concentrations are already causing significant climate changes globally (Lashof and Ahuja, 1990; Solomon et al., 2009; Hansen et al., 2013). An analysis of past conditions in Europe indicates changes in both precipitation and temperature patterns. Northern Europe is experiencing more precipitation, while southern Europe is becoming drier (Gudmundsson and Seneviratne, 2015). An increase in temperature has led to more dry and hot events in recent years compared to the second half of the 20th century (Manning et al., 2019). Climate projections also suggest drier meteorological conditions in Europe in the future (Spinoni et al., 2018). Some studies specifically examine changes in soil moisture trends. According to Samaniego et al. (2018), extreme agricultural drought events are expected to become more frequent, in line with precipitation and temperature projections. Despite its location between the wet north and the dry south, France is projected to experience drying trends in terms of both climatic conditions (Spinoni et al., 2018) and soil moisture (Vidal et al., 2012; Dayon et al., 2018; Soubeyroux et al., 2023). The most severe scenarios are expected to have larger impacts (Dayon et al., 2018).

Several estimates of the impact of climate change on the costs associated with subsidence due to clay shrinkage have been made for France (Gourdier and Plat (2018), Covéa and RiskWeatherTech (2022), and CCR (2023a)). These estimates are based on damage models, which are statistical models used operationally by the insurance industry to estimate losses following a disaster. In cases of subsidence due to clay shrinkage, inputs such as precipitation, temperature, and soil moisture may serve as proxies for weather conditions. Inputs such as clay content may serve as proxies for soil properties. All estimates agree that costs increase as desiccation increases in response to climate warming. The accuracy of these predictions depends on the quality of the inputs.

Clay shrinkage is a significant phenomenon that remains poorly understood at large spatial scales due to the complex soil moisture dynamics and the heterogeneity of clayey soils. Research is currently underway to better understand the drivers of clay shrinkage in order to assist public authorities and the insurance industry. In a previous study (Barthelemy et al., 2023), a yearly drought magnitude index (YDMI) was developed specifically for this hazard, based on soil moisture simulations from the Interactions between Soil, Biosphere, and Atmosphere (ISBA) land surface model. The YDMI quantifies daily soil moisture anomalies summed over a year based on a soil layer at a depth of 0.80 to 1 m. Its characteristics were adjusted by comparison with a sample of insurance claims data.

The objective of this study is to present a retrospective analysis of droughts in France since 2000 and to provide insight into climate warming-induced trends through YDMI. The YDMI is first computed for a historical period (2000-2022) by forcing ISBA with the SAFRAN atmospheric reanalysis. YDMI trends through 2065 in response to global warming are then assessed by forcing ISBA with the outputs of six different climate models under RCP 4.5 and RCP 8.5.

Section 2 presents the data used in this study, including the ISBA land surface model and historical and projected forcing, as well as the methods employed for index calculation and result analysis. The results are presented and described in Section 3, followed by a discussion and comparison with other works in Section 4. Finally, conclusions are drawn in Section 5.

2 Data and methods

This section describes the various surface simulations used and the concept of drought magnitude. The present analysis is summarized as a flowchart in Fig. 1.

100   ## 2.1 The ISBA land surface model

In this study, soil moisture is simulated by ISBA within version 8.1 of the SURFEX (SURFace Externalisée) modeling platform for numerical weather prediction and climate modeling (Masson et al., 2013; Le Moigne et al., 2020). The ISBA model calculates surface water and energy budgets in response to an atmospheric forcing. Soil moisture at a specific time is determined by the balance between water inflows from precipitation and outflows through runoff, infiltration, and
105   evapotranspiration (Noilhan and Planton, 1986; Noilhan and Mahfouf, 1996). The ISBA model covers the entire French metropolitan area on an 8 km grid, totaling 8925 grid points. The SAFRAN-ISBA-MODCOU (SIM) hydrological suite (Habets et al., 2008) is used operationally to monitor water resources, along with a meteorological analysis and a hydrogeological model. In this case, ISBA is used offline, meaning there is no feedback from the surface to the atmosphere. SAFRAN is a mesoscale analysis of near-surface atmospheric variables, including air temperature, air humidity, wind speed, solid and liquid
110   precipitation, and incident solar and infrared radiation fields. It combines surface observations and atmospheric model simulations (Quintana-Seguí et al., 2008; Vidal et al., 2010).

In this study, we employ a multilayer version of ISBA, ISBA-DIF (Boone et al., 2000; Decharme et al., 2011), which uses a diffusive scheme. The soil column is divided into layers, with increasing thicknesses at greater depths, to better represent hydrological processes and the plant root water uptake. This is necessary due to significant water and temperature gradients at
115   the surface, which require a finer mesh. The number of layers considered is proportional to the rooting depth of the vegetation, with a maximum of 10 layers (adding up to 2m depth) for trees. The definition of multiple layers at different depths is relevant because moisture variations depend on both the distance to the surface and the plant root density.

The ISBA model takes into account the influence of soil texture on moisture variations, as described by Decharme et al. (2011), using empirical pedotransfer functions. These functions establish a connection between parameters such as porosity, matric
120   potential at saturation, and saturated hydraulic conductivity with sand and clay fractions. Specifically, the relationships derived from Clapp and Hornberger (1978) by Noilhan and Lacarrère (1995) are used. In this study, soil texture is (1) represented by the clay, sand, and silt contents derived from the Harmonized World Soil Database (HWSD) version 1.2 (Nachtergaele et al., 2012) at a kilometer resolution, and (2) assumed to be uniform throughout the soil column at each grid point.

To account for variability in land cover within a grid cell, ISBA runs separately for 12 patches. These patches include bare
125   soil, rock, permanent snow, and 9 generic plant functional types: deciduous broadleaf trees, evergreen broadleaf trees, coniferous trees, C_3 crops, C_4 crops, irrigated C_4 crops, grassland, tropical grassland, and wetlands (C_3 and C_4 corresponding to different photosynthetic pathways). The separate runs can be aggregated by averaging the output variables and weighting each patch by its respective fraction in the grid cell. The depth of soil in a patch is determined by the rooting depth of the

corresponding vegetation type and may vary from patch to patch. The geographic distribution of the patches and land surface

130   parameters are derived from the ECOCLIMAP-II database at kilometer resolution (Faroux et al., 2013).

The ISBA model includes a representation of photosynthesis using a CO_2-responsive stomatal conductance scheme, ISBA-A-gs (Calvet et al., 1998), because vegetation plays a critical role in near-surface soil moisture variations. This scheme has been improved over time to account for specific plant responses to drought (Calvet, 2000; Calvet et al., 2004). For each plant functional type, the ISBA-A-gs configuration simulates Leaf Area Index (LAI) from modeled leaf biomass, considering the

135   mass-based leaf nitrogen concentration (Calvet and Soussana, 2001). Phenology is driven by photosynthesis, which is affected by soil moisture, leaf temperature, solar radiation, and air humidity. Therefore, all environmental conditions can influence the simulated LAI. The LAI is updated daily. The simulated LAI has been validated at global (Gibelin et al., 2006), continental (Szczypta et al., 2014), and regional (Brut et al., 2009) scales.

2.2 Historical and projected simulations

140   For this study, two different runs of ISBA were conducted, differing mainly in atmospheric forcing: (1) historical simulation, (2) projected simulation.

The historical simulation used the SAFRAN reanalysis to force ISBA with atmospheric data from 2000-2022. The atmospheric variables are available hourly on a regular 8 km grid. In this article, we refer to SAFRAN as a reference for the past climate.

The projected simulation experiment was conducted by forcing ISBA with projected atmospheric forcing developed in the

145   framework of the EXPLORE-2 project (Explore2 - des futurs de l'eau, 2024). The dataset was generated in several steps. Projected greenhouse gas (GHG) concentrations were fed into a selection of global climate models (GCMs) which were coupled to regional climate models (RCMs) through dynamical downscaling, yielding atmospheric variables over a future period. The data were corrected for bias by comparing it with the SAFRAN historical reference reanalysis, using the ADAMONT method (Verfaillie et al., 2017). The GHG trajectories selected were Representative Concentration Pathways

150   (RCPs) 2.6, 4.5, and 8.5 (Moss et al., 2010), and the RCM selection was based on the EURO-CORDEX works (Jacob et al., 2014, 2020; Kotlarski et al., 2014). These simulations cover the period from 2006 to 2100. For this study, we have chosen to use RCP4.5 and RCP8.5 scenarios applied to a set of 6 GCM-RCM combinations (detailed in Table 1), which we will refer to as models. This amounts to a total of 12 simulations, providing a range of estimates. In Explore2, GCM-RCM selection is based on several criteria: availability for several RCPs, realistic behavior over Europe, absence of known errors, consistency

155   of physical processes between GCM and RCM, and conservation of the dispersion modeled by EURO-CORDEX (Robin et al., 2023). As we deal with rising atmospheric concentrations of CO_2, it is important to consider the conflicting effects of CO_2 on vegetation growth. On one hand, increased CO_2 content stimulates photosynthetic activity by increasing the availability of its main substrate, resulting in increased leaf area and plant transpiration. On the other hand, an increase in CO_2 also causes stomata closure, reducing leaf conductance to atmospheric gases and limiting transpiration. Climate change has been shown

160   to have a significant impact on vegetation, as demonstrated by Laanaia et al. (2016) who predicted earlier leaf onset and peak LAI in the future. To reduce uncertainties, we disabled the effect of CO_2 on vegetation in ISBA for the projected simulation

experiment. We only considered data up to 2065, even though the projected forcing was available up to 2100, in order to limit uncertainties. For this experiment, we conducted 12 ISBA runs spanning from 2006 to 2065, divided into three time horizons: near future (2006-2025), future (2026-2045), and distant future (2046-2065).

165 Both experiments provide hourly volumetric soil moisture data for all patches and layers. Volumetric soil moisture is defined as the water content of the soil, expressed in units of volume of water per unit of volume of soil (m^3m^{-3}). Given our focus on long-term drought events, the data's hourly periodicity is unnecessary. Therefore, we can average the hourly soil moisture values to obtain daily values. Local factors such as the presence of trees around the buildings can play a significant role in the subsidence phenomenon during droughts (Freeman et al., 1992; Hawkins, 2013; Page, 1998). The impact of the local land

170 cover variability can be reduced by selecting a single vegetation patch. To conduct a nationwide analysis, we require a patch that exists throughout the entire territory. This limits our options to bare soil, rocks, deciduous broadleaf trees, C_3 crops, C_4 crops, and grassland patches. The patch selection was made by comparing YDMI simulations to insurance subsidence claims using the method developed by Barthelemy et al. (2023), which resulted in choosing the deciduous broadleaf trees patch. The analysis also revealed the highest correlations for deep model layers, leading us to focus on the moisture variations of the

175 model soil layer 8 (at a depth between 0.8 and 1.0 m), as described in Barthelemy et al. (2023). More information on the methodology and results can be found in the Supplement (see Fig. S1).

Therefore, this work will analyze ISBA outputs for the single deciduous broadleaf trees patch configuration, specifically for the 8th model soil layer located at a depth between 0.8 m and 1.0 m. For the present analysis, we have chosen to exclude mountainous areas. The reliability of ISBA simulations in mountainous areas may be lower due to the coarse spatial resolution.

180 Weather conditions can change rapidly in rugged terrain, such as from one valley to another. Additionally, there is a major drawback to applying our method in a mountainous context. The YDMI is calculated from the liquid water content of the soil, which decreases in winter as soil temperatures fall below the freezing level. Liquid soil moisture distributions are biased by this phenomenon, which also affects the index computations. In mainland France, at a depth between 0.8 and 1.0 m, this phenomenon is only present in mountainous areas. These areas are identified by considering a threshold of 1100 m for the grid

185 cell average altitude. We selected this value after analyzing ISBA soil ice patterns. A total of 567 grid cells (6.4%) meeting this condition were filtered out of the 8925 grid points.

2.3 The YDMI

The YDMI is used to characterize drought patterns based on soil moisture variations (Barthelemy et al., 2023). This index calculates the average integral of daily soil moisture in a year under threshold values ranging from the first to the fifth

190 percentiles of the empirical distribution. Although originally designed to characterize clay shrinkage triggering conditions, it can be used more generally to identify long-term drought trends in soils. No fitting to a known statistical law is necessary and this avoids making assumptions about the distribution of soil moisture and its stability under a fluctuating climate.

The two sets of YDMI values are referred to as historical and projected magnitudes. The drought threshold values for the projected simulations are determined by the percentiles of the daily soil moisture distribution for the near future time horizon

195 of 2006-2025 only. The percentiles that define the thresholds are computed separately for each simulation (1 historical and 12 projected simulations), ensuring that droughts that occur with equal frequency are identified, even if the models are biased (Fig. S2). The statement that the longer the period, the more robust the distribution is not applicable in this context due to the hypothesis of a stable soil moisture distribution being irrelevant in the context of climate change. Additionally, basing the reference on the first 20 years allows for the identification of emerging trends during this period. Assuming a fixed definition

200 of drought based on past values implies no adaptation and unchanged vulnerability of assets to drought conditions. This assumption is relevant in the context of clay shrinkage-induced subsidence, which mainly affects already-built homes.

The YDMI result is classified into four classes ranging from no drought (class 0) to extreme drought conditions (class 3). The methodology proposed by Barthelemy et al. (2023) for defining the classes involves sorting all positive YDMI values into three groups of equal size to form classes 1, 2, and 3 of increasing YDMI values, while all null values are assigned to class 0.

205 The zoning of the classes is defined based on the historical YDMI set to ensure consistency between the two experiments.

2.4 Statistical analysis

The analysis focuses on the YDMI values obtained from historical and projected experiments. In section 3.1, we describe the spatial patterns of historical YDMI by commenting on individual maps for each year. Subsequently, we investigate differences in historical and projected YDMI in section 3.2. First, we provide a preliminary assessment by comparing their distributions,

210 while separating them by RCP scenario, model, and time horizon. To investigate trends for each model and scenario, we performed a non-parametric Mann-Kendall test (Wilks, 2011). The null hypothesis associated with this test is the absence of trend, and the resulting p-value indicates the probability of obtaining such an outcome if the null hypothesis were correct. These results provide insight into the statistical significance of patterns in our data. After conducting this model-wise assessment, we compare in each point the third quartile (75th percentile) of YDMI between historical and projected sets,

215 separated by RCP and time horizon. This provides spatialized and robust information on future drought trends. Finally, we assess trends in drought spatial extent by comparing the distribution of model grid cells in each YDMI class annually for each set, RCP scenario, and time horizon. Due to the expected opposite precipitation trends in northern (wetting) and southern (drying) Europe with global warming (Spinoni et al., 2018), we conducted an analysis at the national scale and for the two French regions, Grand Est and Occitanie, located in the North and South of the country, respectively.

220 ## 2.5 NatCat regime

The national natural disaster compensation scheme in France is called "CatNat" (NatCat). It covers major natural disasters, including subsidence caused by clay shrinkage. Homeowners can only be compensated if their municipality is recognized as being in a state of natural disaster with respect to a specific hazard. Municipalities are the smallest French administrative units (there were 34,955 municipalities as of 01/01/2022). This recognition is done through the publication of an official decree for

225 a given year. The criteria for recognition are based on exceptional events, with a return period of more than 10 years, that cause claims to be selected.. On of these criteria relies on ISBA simulations based on a simplified version of the model (Barthelemy

et al., 2023). The CCR website has the details of each decree, including the municipalities that have made the demand and the final decision. These details are available online (https://catastrophes-naturelles.ccr.fr/les-arretes). This paper compares historical YDMI with NatCat recognition requests. The latter are used as a proxy for drought-induced clay shrinkage.

3 Results

3.1 Historical drought magnitudes

Figure 2 shows the YDMI values for the years 2000 to 2022, computed from the ISBA historical simulation. Similar maps, which plot YDMI classes and dominant drought months, are available as Figs. S3 and S4 in the Supplement. The years 2003, 2018, 2019, 2020, and 2022 stand out for their high YDMI values. The 2022 drought event is the most remarkable of the 23-year series, both in terms of its geographic extent and intensity. The southwest region was the most affected. The year 2003 ranked second in terms of impact, affecting the northeast to southwest zones of the country and Brittany. In contrast, the events of 2018 and 2020 were more localized, mainly affecting the central to northeastern regions and, in 2020, the Rhône corridor. In 2019, a central to southwestern area was affected, except for the Cévennes. In addition to these large, widespread droughts, there were also several more localized events, such as the one in Brittany in 2006 or the one in the southeast and Corsica in 2017. This historical analysis allows us to identify 2003, 2018, 2019, 2020, and 2022 as significant drought years and provides a reference for assessing future droughts.

3.2 Projected drought magnitudes

Figure 3 presents the projected distributions of YDMI for different RCP scenarios, models, and time horizons. The gray box encompasses all models. The distribution of historical YDMI is represented by the yellow box labeled 2000-2022. Table 2 provides the values of the third quartile (percentile 75). For the first time horizon (2006-2025) and both RCPs, there are minimal differences between models and historical YDMI values. The results show a divergence with increasing time horizons. Although the distributions vary considerably for each model, the combination of all models indicates an upward trend over time. This effect is more pronounced for RCP8.5 than for RCP4.5. Specifically, the third quartile of YDMI is multiplied by 2 (0.2 to 0.40) for RCP4.5 and by 3 (0.21 to 0.62) for RCP8.5 from the near future to the distant future, considering all models together.

Figure 4 displays the trends in YDMI identified by the Mann-Kendall test for each of the 12 projected simulations processed separately. The different models present contrasting results for both RCPs. Although some punctual decreasing trends are identified, more in RCP 4.5 than in RCP 8.5, patterns of increasing YDMI dominate with higher confidence levels. This is particularly true for the EC-RCA4 and EC-RACM models in RCP 4.5, and models EC_RCA4, MPI_CCLM, and MPI_REMO in RCP 8.5. For RCP4.5, most models identify an increase in the southwestern region of the country, although the affected ISBA grid points rarely overlap between models. For RCP8.5, four out of six models identify a more widespread increase in

the same area, with half of them having higher levels of confidence. In three of the models, the increase extends as far as the northeast, and for MPI-CCLM, it is maximal in the west.

Figure 5 displays the third quartile (75th percentile) of YDMI in each grid cell, combining all models and separating time
260   horizons and RCP. Focusing on the third quartile allows for a more robust analysis of trends in the highest YDMI values of the dataset compared to the maximum. The historical subplot indicates that the southwest and center of France have been the most affected by high YDMI, as observed on the individual maps. There is an observed trend of increasing YDMI over time, as seen across all models. Projections for both scenarios are similar up to 2045, but diverge in the final time horizon of 2046-2065, with RCP8.5 showing a more significant increase. The two scenarios agree on an increase, but on different scales, in
265   southwestern France bordering the Pyrenees, and in eastern France from the Jura to the Vosges. Although we did not anticipate any differences between the YDMI projected for the historical period (2000-2022) and the near-future period (2006-2025), we did observe higher YDMI values in the former.

Figure 6 displays the YDMI class fractional area for each YDMI class, separated by time horizon and RCP scenario, for France, and for the Grand Est and Occitanie regions. It is observed that the proportion of drought-free years tends to decrease with
270   time for both scenarios for France, with the average percentage of grid cells per year in class 0 decreasing from 60% for 2000-2022 to 40% for 2046-2065 RCP8.5. Compared to class 0, the percentage of cells with nonzero YDMI values (classes 1, 2, and 3) increases, particularly for RCP 8.5. Class 3 is the only category defined solely by a lower bound criterion, and therefore it concentrates extreme events, resulting in a high number of outliers. The section 3.1 identifies five notable drought years for the period 2000-2022, which stand out as class 3 outliers: 2022 (with 90% of France in class 3), 2003 (60%), 2020 (50%),
275   2018 (35%), and 2019 (20%). It is worth noting that the historical year 2022 remains unmatched in terms of drought, all models and scenarios considered. The projected class 3 outliers are biased downward compared to the other historical class 3 outlier years (2003, 2020, 2018, 2019). In addition to the observed inconsistency, there are significant differences in the distributions of historical and near-future YDMI values. This finding was unexpected, given the large time overlap (2000-2022 vs. 2006-2025). A higher proportion of null YDMI and lower proportion of nonzero YDMI were found for the historical experiment
280   compared to the projected experiment, which is related to the outlier difference mentioned above. Similar conclusions can be drawn for the Grand Est region (Fig. 6b) and Occitanie (Fig. 6c). During the historical period, Grand Est experienced fewer droughts than Occitanie. However, both regions are projected to experience a drying pattern. This indicates that the differences between historical and projected YDMI are greater for Grand Est than for Occitanie.

4 Discussion

285   The objective of this work is to describe drought trends in France, both in the past and future periods. In the previous section, we presented a retrospective analysis of droughts in France between 2000 and 2022, by calculating YDMI using ISBA and the SAFRAN reanalysis. Five years stand out in order of importance: 2022, 2003, 2020, 2018, and 2019. We then analyzed future YDMI trends until 2065 under RCP 4.5 and RCP 8.5. All models indicate that drought characteristics will worsen in the future,

particularly under RCP 8.5. We discovered unexpected differences between historical and near-future YDMI values. In this
290   section, we will discuss these findings in relation to other studies.

4.1 Is historical YDMI consistent with external sources of information?

To evaluate the significance of the YDMI in monitoring clay shrinkage-induced subsidence, we compare the retrospective
index with the history of issued NatCat recognition requests. Figure 7 compares the distribution of YDMI in France for each
year, sorted into four classes, with the number of NatCat requests issued. It is important to note that drought is not the only
295   factor causing clay shrinkage, as the presence of clay mineral is necessary. Therefore, we do not anticipate a perfect correlation
between the index and the requests. However, it is the most significant factor that changes over time, making year-to-year
comparisons relevant. It is important to note that the comparison is made using the total number of requests, not just the
accepted ones that led to a decree, as one of the recognition criteria is based on ISBA. As explained in the previous section
and illustrated in Fig. 7a and Fig. 7b, the YDMI identifies 2022, 2003, 2020, 2018, and 2019 as significant drought years in
300   order of importance. Figure 7c shows that the highest number of requests are concentrated in these years. Specifically, in 2003
and 2022, there were more than 7500 requests, which is over 20% of all French municipalities. However, it is important to
note that there is a bias in the NatCat dataset as the number of requests issued each year increases with time. For instance,
there were no requests in only two years: 2000 and 2001. Similar drought conditions occurred later in the record (2002, 2004,
2007, 2008, 2014, 2021), but this time they were associated with requests. This phenomenon is widely recognized in the
305   insurance industry. Although the conditions remain the same, the number of requests increases over time due to two reasons:
(1) an increase in awareness of the issue and (2) some municipalities repeat the process each year after their initial request is
denied.

The European Drought Observatory (EDO) is a service provided by the Joint Research Center (JRC) of the European
Commission. Since 2011, it has been reporting on significant drought events in Europe. Each report provides detailed
310   information on the characteristics of the drought event at different levels, including temperature, precipitation, soil moisture,
and vegetation. The assessment of soil moisture is based on simulations performed by the JRC hydrological model LISFLOOD.
To ensure objectivity, we compared our YDMI retrospective with independent reports. Météo-France also conducts similar
studies, but they are based on ISBA simulations. For the period 2011-2022, we collected five reports on the years 2015, 2018,
2019, 2020, and 2022. The 2015 report by Micale et al. (2015) indicates that France, particularly its eastern region, experienced
315   a significant soil moisture deficit during the summer, surpassing that of 2003. In 2018, France experienced a drought that
began in September in the northeast and spread to the rest of the country by the end of the month (Masante et al., 2018). The
2019 report by Masante et al. (2019) describes an event that mainly affected central France. In 2020, the drought episode
centered on France throughout the summer, with the northern half of the country being the most affected (Barbosa et al., 2020).
The 2022 report by Toreti et al. (2022) describes significant soil moisture anomalies throughout the country, which is consistent
320   with our findings. All these works highlight the same drought years, except for 2015. The location of the event also matches,

such as central France in 2020 or the entire country in 2022. However, YDMI values in 2015 do not correspond to the EDO report. The event may have gone undetected due to the drought not propagating in depth this year.

4.2 How can differences between historical and projected YDMI be explained?

Section 3.2 describes the differences between historical and 2006-2025 projected YDMI. These differences were unexpected, because of the time overlap and the weak divergence of CO_2 concentrations in the projected near future. The projected simulations are more pessimistic in the median and more optimistic at the extremes than the historical simulations. The gap in the data may be attributed to differences in climate forcing between reanalysis and climate models, specifically in temperature or precipitation fields. This explanation is plausible, as a recent study by Vautard et al. (2023) demonstrated that CMIP6 climate models had difficulty simulating temperature extremes in Western Europe. Underestimation of high temperatures results in underestimation of drought, as high temperatures drive evaporative fluxes. The reason for the difference may also be found deeper in the modeling process, specifically in the land surface model. The only variation between the simulations is the CO_2 feedback on vegetation, which is enabled for the historical simulation and disabled for the projected simulation. This could lead to a dissimilar vegetation response for the same CO_2 levels. Berg and Sheffield (2018) suggest that failing to account for the impact of CO_2 on plant water use could result in a significant bias in soil moisture fluctuations. Although we previously identified two opposing effects of CO_2 on plant transpiration (Sect. 2.2), reduced stomatal conductance may dominate, resulting in limited transpiration and thus limited soil desiccation.

4.3 What are the sources of uncertainty?

The study's findings are the result of a lengthy modeling process. It is important to interpret them with care, considering the uncertainties associated with each step. These uncertainties are listed below.

4.3.1 Atmospheric forcing errors

The SAFRAN reanalysis utilized as the historical forcing combines observations and model data. Consequently, it may be subject to observational and meteorological model bias, as well as bias due to the coarse grid resolution. Similar limitations can be listed for the projected forcing. It is important to note the individual biases of each GCM and RCM. Theoretically, these biases tend to cancel each other out when using an ensemble of simulations. The ensemble we use has only 6 members. Adding more members, such as GCMs and RCMs, as well as multiple realizations of the same GCMs and RCMs to explore internal variability, would increase the robustness and reliability of the results. The weighting of each model contribution to the ensemble mean could also be considered (Ribes et al., 2021; Ribes et al., 2022). Model-to-model comparisons (as described in section 3.2) have identified trends of varying statistical significance. The climate modeling framework adopted here involves feeding the same CO_2 evolution into a set of models and assessing their response over time. However, it is not stated that all models warm at the same rate. Other approaches exist that take this element into account. For instance, Samaniego et al. (2018) analyze drought as a function of warming instead of time. This choice enhances model consistency and reduces uncertainty.

4.3.2 Model shortcomings

There are several sources of uncertainty associated with ISBA. The coarse model resolution of 8 km × 8 km is the first limitation, as clay shrinkage occurs on a local scale. ISBA provides an averaged meteorological forcing to a grid cell, resulting

355 in model outputs that are correct on average but do not cover the range of possible values found within a real 64 km² square. The patch concept addresses the sub-grid land cover variability by generating as many outputs as there are vegetation types, and a single vegetation patch is used in this study. While vegetation type is a relevant factor contributing to heterogeneity, it is not the only one. At the grid cell scale, there may be several vegetation species of the same type, as well as different soil textures in various vertical combinations. To improve the approach, simulations could be repeated for a wider range of soil

360 and vegetation parameters to better reflect reality. Changes in soil hydromechanical parameters with depth could also be implemented. Several databases such as SoilGrids (ISRIC, 2020) already provide such information of vertical texture variations. A disadvantage of ISBA is that its hydromechanical soil parameters remain stationary and do not change with time. However, the literature has shown that pore structure is affected by both drying-wetting and freeze-thaw cycles (Zhao et al., 2021). This oversimplification misrepresents the actual water content. Additionally, the lack of CO_2 feedback in the projected

365 experiment, mentioned in the previous subsection, contributes to uncertainty. Although ISBA has been validated with in situ data (Decharme et al., 2011), it relies on simplifying assumptions that introduce bias. These assumptions are specific to each model and result from choices made during the design phase. To compensate for individual biases, it would be appropriate to base drought assessments on simulations from multiple land surface models, as done by Samaniego et al. (2018).

4.3.3 The lack of representativeness of the drought index

370 Finally, uncertainty arises from the method used to calculate the drought index. YDMI is an annual index, chosen to give it an operational focus, particularly towards the insurance industry, which mostly operates on a calendar year scale. This approach is consistent with soil moisture variations, as soil moisture periodically decreases each year during the summer season. However, this choice sacrifices our ability to identify and characterize multi-year drought events, which are expected to become more frequent with global warming (Hari et al., 2020). We define drought as occurring when the daily soil moisture value falls

375 within the lowest 1 to 5% relative to a given period. In contrast to the historical experiment, the drought threshold for the projected experiment is defined over the first 20 years (2006-2025). Implicitly, this means that a drought event will always have the same impact, whether it occurs in 2006 or 2065. Regarding clay shrinkage, this hypothesis is realistic because most exposed assets already exist and are at risk. However, it is a particularly pessimistic view that completely ignores the impact of prevention. Preventive measures have recently been implemented to establish rules for the construction of new buildings

380 (LégiFrance, 2018). In the meantime, research initiatives are being undertaken to prevent subsidence damage using various strategies. For instance, some aim to limit shrinkage by injecting resin (Al-Atroush et al., 2021), while others propose maintaining soil hydration during drought events (Ighil Ameur, 2021).

4.4 What are the limitations and possible applications of this work?

One limitation of this analysis is that mountainous areas were removed, which resulted in spatial gaps where clay shrinkage-
385 induced subsidence may occur in limited locations. To address this, soil moisture calculations could be based on total water
content instead of just liquid water content, which would allow these areas to be considered. However, the coarse resolution
of ISBA is still a problem when dealing with rugged terrain and local biophysical processes.

In spite of these limitations, calculating YDMI can help characterize the conditions that cause clay shrinkage and add to our
understanding of the phenomenon. This information is critical for policymakers and the insurance industry to better anticipate
390 and manage the consequences of extreme drought events. The projected assessment is particularly relevant in the context of
global warming. However, YDMI alone cannot be used for this purpose. For a complete assessment, triggering factors must
be combined with the soil predisposing factor. The predisposing factor is the soil's ability to shrink, which is called
susceptibility. Previous studies have provided an analysis of the susceptibility to the shrinkage-swell phenomenon (e.g. Olive
et al., 1989), based on the combination of several predisposing factors, such as: proportion of clay material, heterogeneity of
395 the layers, proportion of minerals susceptible to swelling, swelling-shrinkage intensity of the clay, layer thickness, and
preferential water paths. Future improvements will involve combining the current drought index with BRGM's regional
susceptibility maps. However, there are several challenges to overcome, particularly the spatial heterogeneity of clay deposits
at large scales (Georisques, 2019).

5 Conclusion

400 This paper analyzes past and future drought events in France from 2000 to 2065 that are likely to cause clay shrinkage, using
an adapted index. The YDMI index is based on soil moisture simulations from the ISBA land surface model, which is
successively forced by an atmospheric reanalysis and an ensemble of six climate models. The index characteristics were
adjusted in a previous study (Barthelemy et al., 2023) by comparison with insurance data. The results are as follows:

- Significant soil moisture drought events occurred in France in 2003, 2018, 2019, 2020, and 2022. In 2022, high index
405   values were observed throughout the country.

- Drought characteristics are expected to worsen in the future, particularly under RCP8.5. The scenarios diverge
    significantly after 2046, and both the north and south of the country will be affected.

- Unexpected differences were found between historical and projected indices (projections are more pessimistic on
    average and more optimistic regarding extreme events). These differences may be due to either the climate forcing or
410   the vegetation response of the land surface scheme.

Finally, YDMI quantifies drought on an annual scale for deciduous broadleaf tree vegetation, making it applicable in
agricultural or forest management contexts beyond this specific example. This methodology can be applied to other countries,
as clay shrinkage-induced subsidence is not unique to France. The SURFEX modeling platform that supports ISBA is
applicable anywhere, provided that high-resolution atmospheric forcing is available.

415 **Code availability**

The analysis was carried out with Python codes that can be made available upon request. SURFEX can be downloaded freely at http://www.umr-cnrm.fr/surfex/data/OPEN-SURFEX/open_surfex_v8_1_20210914.tar.gz (CNRM, 2016). It is provided under a CECILL-C license (French equivalent to the LGPL license).

Data availability

420 The data presented in the Figures are available online at:

Supplement

The supplement related to this article is available online at:

Author contributions

SBa and JCC designed the experiments. SBa performed the investigation, did the formal analysis and wrote the paper. BB did
425 the historical simulations. MTB did the projected simulations. All co-authors participated in the interpretation of the results and the revision of the paper.

Competing interests

The contact author has declared that none of the authors has any competing interests.

Acknowledgments

430 The authors would like to thank the operational services of Météo-France (DCSC).

Financial support

The PhD thesis work of Sophie Barthelemy was co-funded by BRGM (Bureau de Recherches Géologiques et Minières), CCR (Caisse Centrale de Réassurance) and Météo-France.

435 **References**

Al-Atroush, M. E., Shabbir, O., Almeshari, B., Waly, M., and Sebaey, T. A.: A Novel Application of the Hydrophobic Polyurethane Foam: Expansive Soil Stabilization, Polymers, 13, 1335, https://doi.org/10.3390/polym13081335, 2021.

440 Barbosa, P., Masante, D., Arias Muños, C., Cammalleri, C., de Jager, A., Magni, D., Mazzeschi, M., McCormick, N., Naumann, G., Spinoni, J., and Vogt, J.: Drought in Europe September 2020, Publications Office of the European Union, Available at: https://edo.jrc.ec.europa.eu/documents/news/EDODroughtNews202009_Europe.pdf (last access: 27 February 2024), 2020.

445 Barthelemy, S., Bonan, B., Calvet, J.-C., Grandjean, G., Kapsambelis, D., and Bernardie, S.: A new approach for drought index adjustment to clay-shrinkage-induced subsidence over France: advantages of the interactive leaf area index, Nat. Hazards Earth Syst. Sci., 24, 999–1016, https://doi.org/10.5194/nhess-24-999-2024, 2024.

Berg, A. and Sheffield, J.: Climate Change and Drought: the Soil Moisture Perspective, Curr. Clim. Change Rep., 4, 180–191, https://doi.org/10.1007/s40641-018-0095-0, 2018.

450
Boone, A., Masson, V., Meyers, T., and Noilhan, J.: The Influence of the Inclusion of Soil Freezing on Simulations by a Soil–Vegetation–Atmosphere Transfer Scheme, J. Appl. Meteorol., 39, 1544–1569, https://doi.org/10.1175/1520-0450(2000)039<1544:TIOTIO>2.0.CO;2, 2000.

455 Brut, A., Rüdiger, C., Lafont, S., Roujean, J. L., Calvet, J. C., Jarlan, L., Gibelin, A. L., Albergel, C., Le Moigne, P., Soussana, J. F., Klumpp, K., Guyon, D., Wigneron, J. P., and Ceschia, E.: Modelling LAI at a regional scale with ISBA-A-gs: Comparison with satellite-derived LAI over southwestern France, Biogeosciences, 6, 1389–1404, https://doi.org/10.5194/bg-6-1389-2009, 2009.

460 Calvet, J.-C.: Investigating soil and atmospheric plant water stress using physiological and micrometeorological data, Agric. For. Meteorol., 103, 229–247, https://doi.org/10.1016/S0168-1923(00)00130-1, 2000.

Calvet, J.-C. and Soussana, J.-F.: Modelling CO_2-enrichment effects using an interactive vegetation SVAT scheme, Agric. For. Meteorol., 108, 129–152, https://doi.org/10.1016/S0168-1923(01)00235-0, 2001.

465
Calvet, J.-C., Noilhan, J., Roujean, J.-L., Bessemoulin, P., Cabelguenne, M., Olioso, A., and Wigneron, J.-P.: An interactive vegetation SVAT model tested against data from six contrasting sites, Agric. For. Meteorol., 92, 73–95, https://doi.org/10.1016/S0168-1923(98)00091-4, 1998.

470 Calvet, J.-C., Rivalland, V., Picon-Cochard, C., and Guehl, J.-M.: Modelling forest transpiration and CO_2 fluxes—response to soil moisture stress, Agric. For. Meteorol., 124, 143–156, https://doi.org/10.1016/j.agrformet.2004.01.007, 2004.

CCR: Conséquences du changement climatique sur le coût des catastrophes naturelles en France à horizon 2050, Available at: https://www.ccr.fr/documents/35794/1255983/CCR+Etude+climat+BAG+23102023+page+22mo.pdf/68b95f6e-8238-4dcc-6c56-025fa410257b?t=1698161402128 (last access: 27 February 2024), 2023a.

475

CCR: Les Catastrophes Naturelles en France Bilan 1982-2022, Available at: https://catastrophes-naturelles.ccr.fr/documents/148935/368920/BILAN+Cat+Nat+2022_HD_12062023.pdf/5b5397f0-2118-2252-608f-76ece6e195a1?t=1686731142230 (last access: 27 February 2024), 2023b.

480
Ciais, Ph., Reichstein, M., Viovy, N., Granier, A., Ogée, J., Allard, V., Aubinet, M., Buchmann, N., Bernhofer, Chr., Carrara, A., Chevallier, F., De Noblet, N., Friend, A. D., Friedlingstein, P., Grünwald, T., Heinesch, B., Keronen, P., Knohl, A., Krinner, G., Loustau, D., Manca, G., Matteucci, G., Miglietta, F., Ourcival, J. M., Papale, D., Pilegaard, K., Rambal, S., Seufert, G., Soussana, J. F., Sanz, M. J., Schulze, E. D., Vesala, T., and Valentini, R.: Europe-wide reduction in primary
485 productivity caused by the heat and drought in 2003, Nature, 437, 529–533, https://doi.org/10.1038/nature03972, 2005.

Clapp, R. B. and Hornberger, G. M.: Empirical equations for some soil hydraulic properties, Water Resour. Res., 14, 601–604, https://doi.org/10.1029/WR014i004p00601, 1978.

490 Covéa and RiskWeatherTech: Changement climatique et Assurance: Quelles conséquences sur la sinistralité à horizon 2050?, Available at : https://www.covea.com/sites/default/files/2022-02/202202_Livre_Blanc_Cov%C3%A9a_Risques_Climatiques.pdf (last access: 27 February 2024), 2022.

Dayon, G., Boé, J., Martin, É., and Gailhard, J.: Impacts of climate change on the hydrological cycle over France and
495 associated uncertainties, Comptes Rendus - Geosci., 350, 141–153, https://doi.org/10.1016/j.crte.2018.03.001, 2018.

Decharme, B., Boone, A., Delire, C., and Noilhan, J.: Local evaluation of the Interaction between Soil Biosphere Atmosphere soil multilayer diffusion scheme using four pedotransfer functions, J. Geophys. Res. Atmospheres, 116, 1–29, https://doi.org/10.1029/2011JD016002, 2011.
500
Dirmeyer, P. A., Balsamo, G., Blyth, E. M., Morrison, R., and Cooper, H. M.: Land-Atmosphere Interactions Exacerbated the Drought and Heatwave Over Northern Europe During Summer 2018, AGU Adv., 2, e2020AV000283, https://doi.org/10.1029/2020AV000283, 2021.

505 Explore2 - des futurs de l'eau: https://professionnels.ofb.fr/fr/node/1244, last access: 27 February 2024.

Faroux, S., Kaptué Tchuenté, A. T., Roujean, J.-L., Masson, V., Martin, E., and Le Moigne, P.: ECOCLIMAP-II/Europe: a twofold database of ecosystems and surface parameters at 1 km resolution based on satellite information for use in land surface, meteorological and climate models, Geosci. Model Dev., 6, 563–582, https://doi.org/10.5194/gmd-6-563-2013,
510 2013.

Freeman, T. J., Burford, D., and Crilly, M. S.: Seasonal foundation movements in London Clay, in: Proceedings of the 4th International Conference on Ground Movements and Structures, Cardiff, UK, 8–11 July 1991, 485–501, 1992.

515 Georisques: Dossier expert sur le retrait-gonflement des argiles – Exposition du territoire au phénomène, https://www.georisques.gouv.fr/articles-risques/retrait-gonflement-des-argiles/exposition-du-territoire-au-phenomene (last access: 2 April 2024), 2019.

Gibelin, A. L., Calvet, J. C., Roujean, J. L., Jarlan, L., and Los, S. O.: Ability of the land surface model ISBA-A-gs to
520 simulate leaf area index at the global scale: Comparison with satellites products, J. Geophys. Res. Atmospheres, 111, https://doi.org/10.1029/2005JD006691, 2006.

Gleick, P. H., Pacific Institute for Studies in Development, Environment, and Security, Stockholm Environment Institute, and Pacific Institute for Studies in Development, Environment, and Security (Eds.): Water in crisis: a guide to the world's
525 fresh water resources, Oxford Univ. Press, New York, NY, 473 pp., ISBN 978-0-19-507628-8, 1993.

Gourdier, S. and Plat, E. : Impact du changement climatique sur la sinistralité due au retrait-gonflement des argiles. Journées Nationales de Géotechnique et Géologie de l'Ingénieur (JNGG), Champs-sur-Marne, France, https://brgm.hal.science/hal-01768395/ (last access: 27 February 2024), 2018.
530
Gudmundsson, L. and Seneviratne, S. I.: European drought trends, Proc. Int. Assoc. Hydrol. Sci., 369, 75–79, https://doi.org/10.5194/piahs-369-75-2015, 2015.

Habets, F., Boone, A., Champeaux, J. L., Etchevers, P., Franchistéguy, L., Leblois, E., Ledoux, E., Le Moigne, P., Martin,
535 E., Morel, S., Noilhan, J., Seguí, P. Q., Rousset-Regimbeau, F., and Viennot, P.: The SAFRAN-ISBA-MODCOU

hydrometeorological model applied over France, J. Geophys. Res. Atmospheres, 113, 1–18, https://doi.org/10.1029/2007JD008548, 2008.

540 Hansen, J., Kharecha, P., Sato, M., Masson-Delmotte, V., Ackerman, F., Beerling, D.J., Hearty, P.J., Hoegh-Guldberg, O., Hsu, S.-L., and Parmesan, C.: Assessing "dangerous climate change": required reduction of carbon emissions to protect young people, future generations and nature, PLoS ONE, 8, e81648, https://doi.org/10.1371/journal.pone.0081648, 2013.

Hari, V., Rakovec, O., Markonis, Y., Hanel, M., and Kumar, R.: Increased future occurrences of the exceptional 2018–2019 Central European drought under global warming, Sci. Rep., 10, 12207, https://doi.org/10.1038/s41598-020-68872-9, 2020.

545

Hawkins, A. B.: Some engineering geological effects of drought: Examples from the UK, Bull. Eng. Geol. Environ., 72, 37–59, https://doi.org/10.1007/s10064-013-0458-7, 2013.

Ighil Ameur, L.: Experimental Analysis of Shrinkage-swelling Phenomenon of Clays Application to an Individual House
550 Affected by Drought Under Climate Change Effects, ASCE EMI/PMC, Available at: https://www.researchgate.net/publication/356284599_Experimental_Analysis_of_Shrinkage-swelling_Phenomenon_of_Clays_-_Application_to_an_Individual_House_Affected_by_Drought_Under_Climate_Change_Effects (last access: 27 February 2024), 2021.

555

ISRIC: SoilGrids — global gridded soil information, https://www.isric.org/explore/soilgrids (last access: 2 April 2024), 2020.

Jacob, D., Petersen, J., Eggert, B., Alias, A., Christensen, O. B., Bouwer, L. M., Braun, A., Colette, A., Déqué, M.,
560 Georgievski, G., Georgopoulou, E., Gobiet, A., Menut, L., Nikulin, G., Haensler, A., Hempelmann, N., Jones, C., Keuler, K., Kovats, S., Kröner, N., Kotlarski, S., Kriegsmann, A., Martin, E., van Meijgaard, E., Moseley, C., Pfeifer, S., Preuschmann, S., Radermacher, C., Radtke, K., Rechid, D., Rounsevell, M., Samuelsson, P., Somot, S., Soussana, J.-F., Teichmann, C., Valentini, R., Vautard, R., Weber, B., and Yiou, P.: EURO-CORDEX: new high-resolution climate change projections for European impact research, Reg. Environ. Change, 14, 563–578, https://doi.org/10.1007/s10113-013-0499-2, 2014.

565

Jacob, D., Teichmann, C., Sobolowski, S., Katragkou, E., Anders, I., Belda, M., Benestad, R., Boberg, F., Buonomo, E., Cardoso, R. M., Casanueva, A., Christensen, O. B., Christensen, J. H., Coppola, E., De Cruz, L., Davin, E. L., Dobler, A., Domínguez, M., Fealy, R., Fernandez, J., Gaertner, M. A., García-Díez, M., Giorgi, F., Gobiet, A., Goergen, K., Gómez-Navarro, J. J., Alemán, J. J. G., Gutiérrez, C., Gutiérrez, J. M., Güttler, I., Haensler, A., Halenka, T., Jerez, S., Jiménez-
570 Guerrero, P., Jones, R. G., Keuler, K., Kjellström, E., Knist, S., Kotlarski, S., Maraun, D., van Meijgaard, E., Mercogliano, P., Montávez, J. P., Navarra, A., Nikulin, G., de Noblet-Ducoudré, N., Panitz, H.-J., Pfeifer, S., Piazza, M., Pichelli, E., Pietikäinen, J.-P., Prein, A. F., Preuschmann, S., Rechid, D., Rockel, B., Romera, R., Sánchez, E., Sieck, K., Soares, P. M. M., Somot, S., Srnec, L., Sørland, S. L., Termonia, P., Truhetz, H., Vautard, R., Warrach-Sagi, K., and Wulfmeyer, V.: Regional climate downscaling over Europe: perspectives from the EURO-CORDEX community, Reg. Environ. Change, 20,
575 51, https://doi.org/10.1007/s10113-020-01606-9, 2020.

Kotlarski, S., Keuler, K., Christensen, O. B., Colette, A., Déqué, M., Gobiet, A., Goergen, K., Jacob, D., Lüthi, D., van Meijgaard, E., Nikulin, G., Schär, C., Teichmann, C., Vautard, R., Warrach-Sagi, K., and Wulfmeyer, V.: Regional climate modeling on European scales: a joint standard evaluation of the EURO-CORDEX RCM ensemble, Geosci. Model Dev., 7,
580 1297–1333, https://doi.org/10.5194/gmd-7-1297-2014, 2014.

Laanaia, N., Carrer, D., Calvet, J.-C., and Pagé, C.: How will climate change affect the vegetation cycle over France? A generic modeling approach, Clim. Risk Manag., 13, 31–42, https://doi.org/10.1016/j.crm.2016.06.001, 2016.

585 Lashof, D.A., and Ahuja, D.R.: Relative contributions of greenhouse gas emissions to global warming, Nature, 344, 529–

531, https://doi.org/10.1038/344529a0, 1990.

Le Moigne, P., Besson, F., Martin, E., Boé, J., Boone, A., Decharme, B., Etchevers, P., Faroux, S., Habets, F., Lafaysse, M., Leroux, D., and Rousset-Regimbeau, F.: The latest improvements with SURFEX v8.0 of the Safran-Isba-Modcou hydrometeorological model for France, Geosci. Model Dev., 13, 3925–3946, https://doi.org/10.5194/gmd-13-3925-2020, 2020.

Légifrance: Loi n° 2018-1021 du 23 novembre 2018 portant évolution du logement, de l'aménagement et du numérique, 2018-1021. Available at: https://www.legifrance.gouv.fr/loda/id/JORFTEXT000037639478 (last access: 2 April 2024), 2018.

Manning, C., Widmann, M., Bevacqua, E., Van Loon, A. F., Maraun, D., and Vrac, M.: Increased probability of compound long-duration dry and hot events in Europe during summer (1950–2013), Environ. Res. Lett., 14, 094006, https://doi.org/10.1088/1748-9326/ab23bf, 2019.

Masante, D., Vogt, J., Cammalleri, C., Spinoni, J., and Barbosa, P.: Drought in Central-Northern Europe - September 2018, Publications Office of the European Union, Available at: https://edo.jrc.ec.europa.eu/documents/news/EDODroughtNews201809_Central_North_Europe.pdf (last access: 27 February 2024), 2018.

Masante, D., Barbosa, P., and Magni, D.: Drought in Europe August 2019, Publications Office of the European Union, Available at: https://edo.jrc.ec.europa.eu/documents/news/EDODroughtNews201908_Europe.pdf (last access: 27 February 2024), 2019.

Masson, V., Le Moigne, P., Martin, E., Faroux, S., Alias, A., Alkama, R., Belamari, S., Barbu, A., Boone, A., Bouyssel, F., Brousseau, P., Brun, E., Calvet, J. C., Carrer, D., Decharme, B., Delire, C., Donier, S., Essaouini, K., Gibelin, A. L., Giordani, H., Habets, F., Jidane, M., Kerdraon, G., Kourzeneva, E., Lafaysse, M., Lafont, S., Lebeaupin Brossier, C., Lemonsu, A., Mahfouf, J. F., Marguinaud, P., Mokhtari, M., Morin, S., Pigeon, G., Salgado, R., Seity, Y., Taillefer, F., Tanguy, G., Tulet, P., Vincendon, B., Vionnet, V., and Voldoire, A.: The SURFEXv7.2 land and ocean surface platform for coupled or offline simulation of earth surface variables and fluxes, Geosci. Model Dev., 6, 929–960, https://doi.org/10.5194/gmd-6-929-2013, 2013.

Meisina, C., Zucca, F., Fossati, D., Ceriani, M., and Allievi, J.: Ground deformation monitoring by using the Permanent Scatterers Technique: The example of the Oltrepo Pavese (Lombardia, Italy), Eng. Geol., 88, 240–259, https://doi.org/10.1016/j.enggeo.2006.09.010, 2006.

Micale, F., Vogt, J., and Cammalleri, C.: European Drought Observatory (EDO) Drought News August 2015, Publications Office of the European Union, Available at: https://edo.jrc.ec.europa.eu/documents/news/EDODroughtNews201508.pdf (last access: 27 February 2024), 2015.

Moravec, V., Markonis, Y., Rakovec, O., Svoboda, M., Trnka, M., Kumar, R., and Hanel, M.: Europe under multi-year droughts: how severe was the 2014–2018 drought period?, Environ. Res. Lett., 16, 034062, https://doi.org/10.1088/1748-9326/abe828, 2021.

Moss, R. H., Edmonds, J. A., Hibbard, K. A., Manning, M. R., Rose, S. K., van Vuuren, D. P., Carter, T. R., Emori, S., Kainuma, M., Kram, T., Meehl, G. A., Mitchell, J. F. B., Nakicenovic, N., Riahi, K., Smith, S. J., Stouffer, R. J., Thomson, A. M., Weyant, J. P., and Wilbanks, T. J.: The next generation of scenarios for climate change research and assessment, Nature, 463, 747–756, https://doi.org/10.1038/nature08823, 2010.

Mostafiz, R. B., Friedland, C. J., Rohli, R. V., Bushra, N., and Held, C. L.: Property Risk Assessment for Expansive Soils in

Louisiana, Front. Built Environ., 7, 1–10, https://doi.org/10.3389/fbuil.2021.754761, 2021.

MTES: Cartographie de l'exposition des maisons individuelles au retrait-gonflement des argiles, Available at:
https://www.statistiques.developpement-durable.gouv.fr/sites/default/files/2021-
640   06/note_methode_croisement_retrait_gonflement_argiles_juin2021v3.pdf (last access: 27 February 2024), 2021.

Nachtergaele, F., Velthuizen, H., Verelst, L., and Wiberg, D.: Harmonized World Soil Database Version 1.2, Available at:
https://esdac.jrc.ec.europa.eu/ESDB_Archive/Soil_Data/Docs_GlobalData/Harmonized_World_Soi_Database_v1.2.pdf (last
access: 27 February 2024), 2012.
645
Noilhan, J. and Lacarrère, P.: GCM Grid-Scale Evaporation from Mesoscale Modeling, J. Clim., 8, 206–223,
https://doi.org/10.1175/1520-0442(1995)008<0206:GGSEFM>2.0.CO;2, 1995.

Noilhan, J. and Mahfouf, J.-F.: The ISBA land surface parameterisation scheme, Global Planet. Change, 13, 145–159,
650   https://doi.org/10.1016/0921-8181(95)00043-7, 1996.

Noilhan, J. and Planton, S.: A simple parameterization of land surface processes for meteorological models, Mon. Weather
Rev., 117, 536–549, 1989.
Olive, W. W., Chleborad, A. F., Frahme, C. W., Schlocker, J., Schneider, R. R., and Schuster, R. L.: Swelling clays map of
655   the conterminous United States, https://doi.org/10.3133/i1940, 1989.

Page, R. C. J.: Reducing the cost of subsidence damage despite global warming, Struct. Surv., 16, 67–75,
https://doi.org/10.1108/02630809810219641, 1998.

660   Ribes, A., Boé, J., Qasmi, S., Dubuisson, B., Douville, H., and Terray, L.: An updated assessment of past and future
warming over France based on a regional observational constraint, Earth Syst. Dynam., 13, 1397–1415,
https://doi.org/10.5194/esd-13-1397-2022, 2022.

Ribes, A., Qasmi S., and Gillett N. P.: Making climate projections conditional on historical observations. Sci. Adv., 7,
665   eabc0671, https://doi.org/10.1126/sciadv.abc0671, 2021.

Robin, Y., Corre, L., Marson, P., Bernus, S., Vrac, M., and Thao, S.: Projections climatiques régionalisées : correction de
biais et changements futurs. Available at:
https://entrepot.recherche.data.gouv.fr/file.xhtml?persistentId=doi:10.57745/99X4CD (last access: 27 February 2024), 2023.
670
Quintana-Seguí, P., Le Moigne, P., Durand, Y., Martin, E., Habets, F., Baillon, M., Canellas, C., Franchisteguy, L., and
Morel, S.: Analysis of near-surface atmospheric variables: Validation of the SAFRAN analysis over France, J. Appl.
Meteorol. Climatol. 47, 92–107, https://doi.org/10.1175/2007JAMC1636.1, 2008.

675   Samaniego, L., Thober, S., Kumar, R., Wanders, N., Rakovec, O., Pan, M., Zink, M., Sheffield, J., Wood, E. F., and Marx,
A.: Anthropogenic warming exacerbates European soil moisture droughts, Nat. Clim. Change, 8, 421–426,
https://doi.org/10.1038/s41558-018-0138-5, 2018.

Seneviratne, S. I., Corti, T., Davin, E. L., Hirschi, M., Jaeger, E. B., Lehner, I., Orlowsky, B., and Teuling, A. J.:
680   Investigating soil moisture–climate interactions in a changing climate: A review, Earth-Sci. Rev., 99, 125–161,
https://doi.org/10.1016/j.earscirev.2010.02.004, 2010.

Solomon, S., Plattner, G.-K., Knutti, R., and Friedlingstein, P.: Irreversible climate change due to carbon dioxide emissions.
Proc. Natl. Acad. Sci. USA, 106, 1704–1709, https://doi.org/10.1073/pnas.0812721106, 2009.
685

Soubeyroux, M., Grigis, L., Rousset, F., Corre, L., and Boe, J.: Evolution des sécheresses météorologiques et agricoles en France en contexte de changement climatique, 36th Conference of the International Association of Climatology, Available at: https://drive.google.com/file/d/1Fw18eT6FZz756wwla0vh5Rhxy6XwpNYt/view (last access: 27 February 2024), 2023.

690 Soubeyroux, J.-M., Vidal, J.-P., Najac, J., Kitova, N., Blanchard, M., Dandin, P., Martin, E., Pagé, C., Habets, F. : Projet ClimSec : Impact du changement climatique en France sur la sécheresse et l'eau du sol. Rapport final du projet, https://www.umr-cnrm.fr/IMG/pdf/2011_fmaif_rapport_final_v2.2.pdf (last access: 27 February 2024), 2011.

Spinoni, J., Vogt, J. V., Naumann, G., Barbosa, P., and Dosio, A.: Will drought events become more frequent and severe in
695 Europe?, Int. J. Climatol., 38, 1718–1736, https://doi.org/10.1002/joc.5291, 2018.

Szczypta, C., Calvet, J. C., Maignan, F., Dorigo, W., Baret, F., and Ciais, P.: Suitability of modelled and remotely sensed essential climate variables for monitoring Euro-Mediterranean droughts, Geosci. Model Dev., 7, 931–946, https://doi.org/10.5194/gmd-7-931-2014, 2014.
700

Toreti, A., Bavera, D., Acosta Navarro, J., Cammalleri, C., de Jager, A., Di Ciollo, C. i, Hrast Essenfelder, A., Maetens, W., Masante, D., Magni, D., Mazzeschi, M., and Spinoni, J.: Drought in Europe - August 2022, JRC Global Drought Observatory, https://doi.org/10.2760/264241, 2022.

705 Tzampoglou, P., Loukidis, D., and Koulermou, N.: Seasonal Ground Movement Due to Swelling/Shrinkage of Nicosia Marl, Remote Sens., 14, 1440, https://doi.org/10.3390/rs14061440, 2022.

Vautard, R., Cattiaux, J., Happé, T., Singh, J., Bonnet, R., Cassou, C., Coumou, D., D'Andrea, F., Faranda, D., Fischer, E., Ribes, A., Sippel, S., and Yiou, P.: Heat extremes in Western Europe increasing faster than simulated due to atmospheric
710 circulation trends, Nat. Commun., 14, 6803, https://doi.org/10.1038/s41467-023-42143-3, 2023.

Verfaillie, D., Déqué, M., Morin, S., and Lafaysse, M.: The method ADAMONT v1.0 for statistical adjustment of climate projections applicable to energy balance land surface models, Geosci. Model Dev., 10, 4257–4283, https://doi.org/10.5194/gmd-10-4257-2017, 2017.
715

Vidal, J.-P., Martin, E., Franchistéguy, L., Baillon, M., and Soubeyroux, J.-M.: A 50-year high-resolution atmospheric reanalysis over France with the Safran system, Int. J. Climatol., 30, 1627–1644, https://doi.org/10.1002/joc.2003, 2010.

Vidal, J.-P., Martin, E., Kitova, N., Najac, J., and Soubeyroux, J.-M.: Evolution of spatio-temporal drought characteristics:
720 validation, projections and effect of adaptation scenarios, Hydrol. Earth Syst. Sci., 16, 2935–2955, https://doi.org/10.5194/hess-16-2935-2012, 2012.

Vincent, M., Cojean, R., Fleureau, J.-M., Cui, Y. J., Jacquard, C., Kazmierczak, J.-B., Masrouri, F., Tessier, D., Alimi-Ichola, I., Magnan, J.-P., Blanchard, M., Fabre, D., Pantet, A., Audiguier, M., Plat, E., Souli, H., Taibi, S., Tang, A.-M.,
725 Morlock, C., Maison, T., Mrad, M., Bréda, N., Djeran-Maigre, I., Duc, M., Soubeyroux, J.-M., Denis, A., Proust, D., Geremew, Z., Le Roy, S., Dumont, M., Hemmati, S., Nowamooz, H., Coquet, Y., Pothier, C., Makki, L., Chrétien, M., Fontaine, C. : Rapport de synthèse final du projet ARGIC (Analyse du retrait-gonflement et de ses Incidences sur les Constructions), Projet ANR-05-PRGCU-005, BRGM/RP-57011-FR report, http://infoterre.brgm.fr/rapports/RP-57011-FR.pdf (last access: 27 February 2024), 2009.
730

Wilks, D. S.: Statistical methods in the atmospheric sciences, 3rd ed., Elsevier/Academic Press, Amsterdam ; Boston, 676 pp., ISBN 13: 978-0-12-751966-1, 2011.

Zhao, G., Zou, W., Han, Z., Wang, D., and Wang, X.: Evolution of soil-water and shrinkage characteristics of an expansive
735 clay during freeze-thaw and drying-wetting cycles, Cold Reg. Sci. Technol., 186, 103275,

https://doi.org/10.1016/j.coldregions.2021.103275, 2021.

740 **Table 1: Six GCM-RCM atmospheric model combinations selected as forcing for the projected YDMI derived from the simulations of the ISBA land surface model.**

GCM-RCM atmospheric model combinations	GCM	RCM
CNRM-ALAD	CNRM-CM5	ALADIN63
CNRM-RACM	CNRM-CM5	RACMO22E
EC-RACM	EC-EARTH	RACMO22E
EC-RCA4	EC-EARTH	RCA4
MPI-CCLM	MPI-ESM	CCLM4-8-17
MPI-REMO	MPI-ESM	REMO2009

745

Table 2: Third quartile (75th percentile) of historical and projected YDMI statistical distribution for RCP 4.5 and RCP8.5, separating time horizons and atmospheric models. YDMI values larger or equal to 0.4 are in bold.

Atmospheric forcing		2000-2022	2006-2025	2026-2045	2046-2065
SAFRAN (historical)		0.18			
RCP 4.5	**Pooled data from the 6 models**		0.20	0.29	**0.40**
	CNRM_ALAD		0.24	**0.62**	0.27
	CNRM_RACM		0.24	**0.77**	0.33
	EC_RAC4		0.15	0.04	**0.75**
	EC_RACM		0.15	0.03	**0.76**
	MPI_CCLM		0.23	0.32	0.29
	MPI_REMO		0.20	0.33	0.19
RCP 8.5	**Pooled data from the 6 models**		0.21	0.28	**0.62**
	CNRM_ALAD		0.22	0.16	0.22
	CNRM_RACM		0.25	0.05	0.25
	EC_RAC4		0.15	0.16	**0.70**
	EC_RACM		0.19	0.15	**0.40**
	MPI_CCLM		0.24	**0.91**	1.61
	MPI_REMO		0.22	**0.59**	0.99
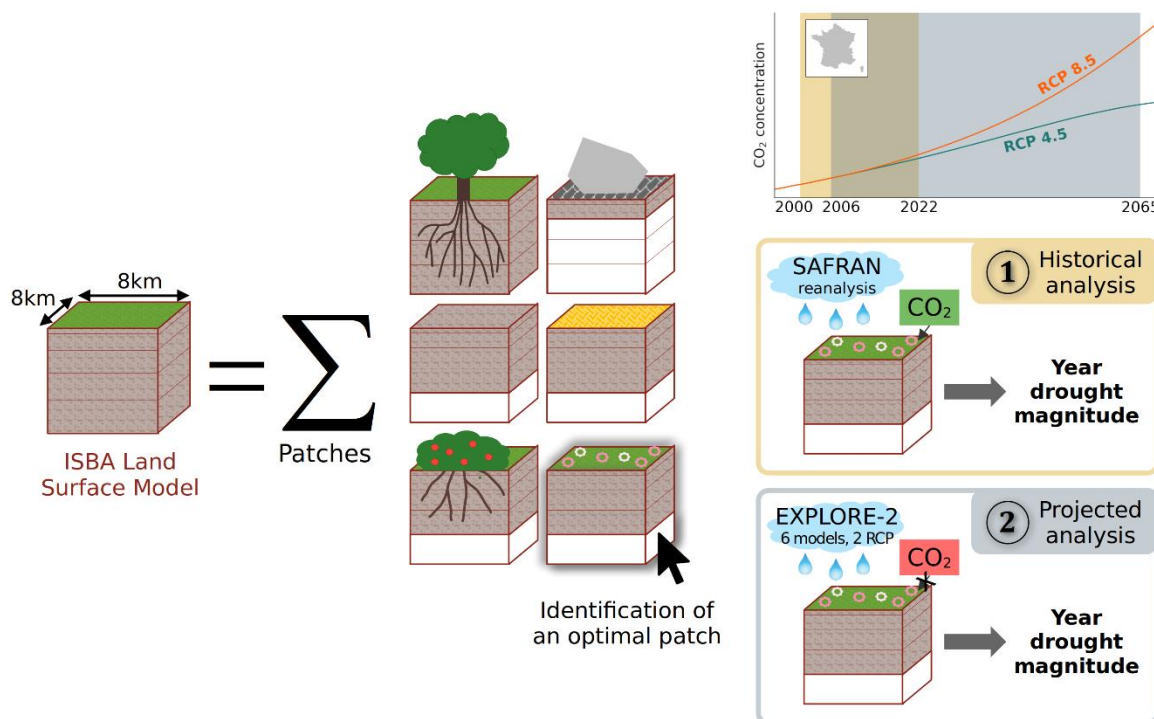
750

Figure 1: Flowchart of the methodology deployed in this study with focus on vegetation patch selection and historical vs. projected analyses.
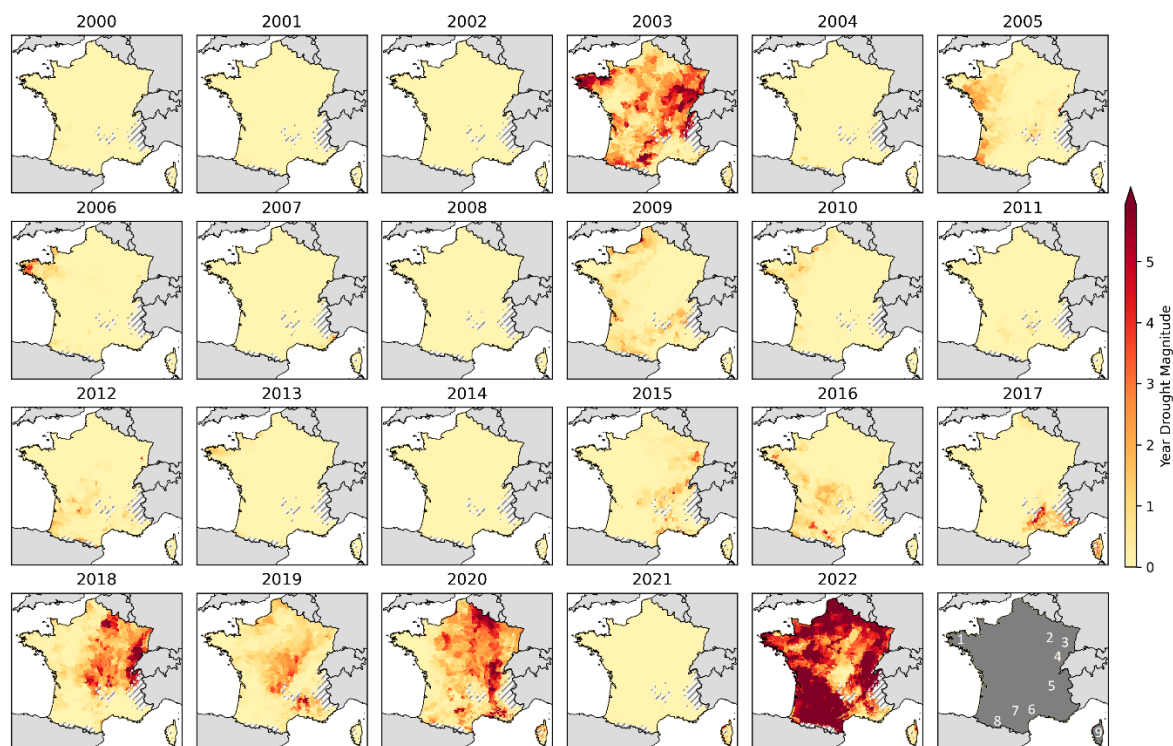
Figure 2: Year drought magnitudes for years 2000 to 2022, computed over France in each grid cell from the ISBA historical simulation. Areas with gray hatching correspond to filtered mountain areas (average altitude > 1100 meters). In the bottom-right subfigure the following areas are indicated by numbers, from 1 to 9: Brittany ("1"), Grand Est ("2", also see Fig. 6), Vosges ("3"), Jura ("4"), Rhône corridor ("5"), Cévennes ("6"), Occitanie ("7", also see Fig. 6), Pyrénées ("8"), and Corsica ("9").
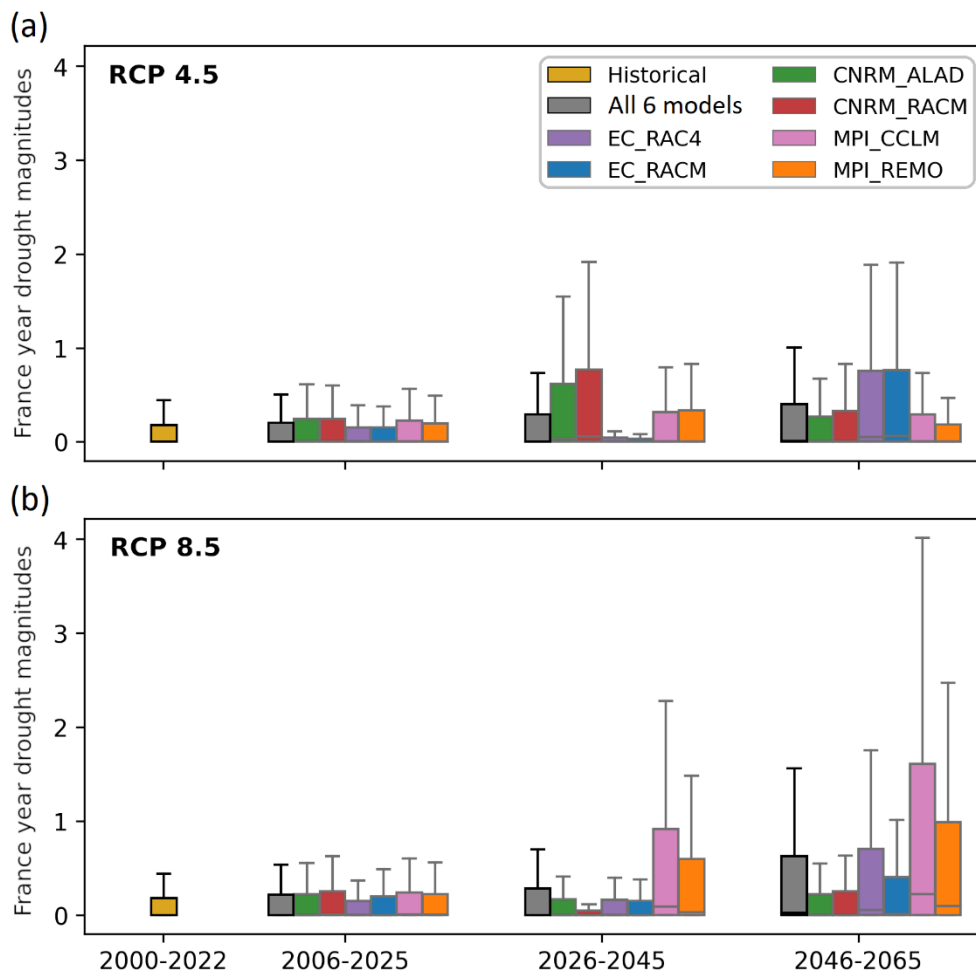
Figure 3: Projected YDMI distributions for (a) RCP 4.5 and (b) RCP8.5, separating time horizons and models. The grey box corresponds to the distribution of all models combined. The distribution of historical magnitudes is plotted as well (yellow box) for comparison. Box edges and center correspond to 25%, 75% and 50% percentiles. Whiskers extend to 1.5 times the interquartile range, equal to the difference between 75% and 25% percentiles. Outliers are not displayed.
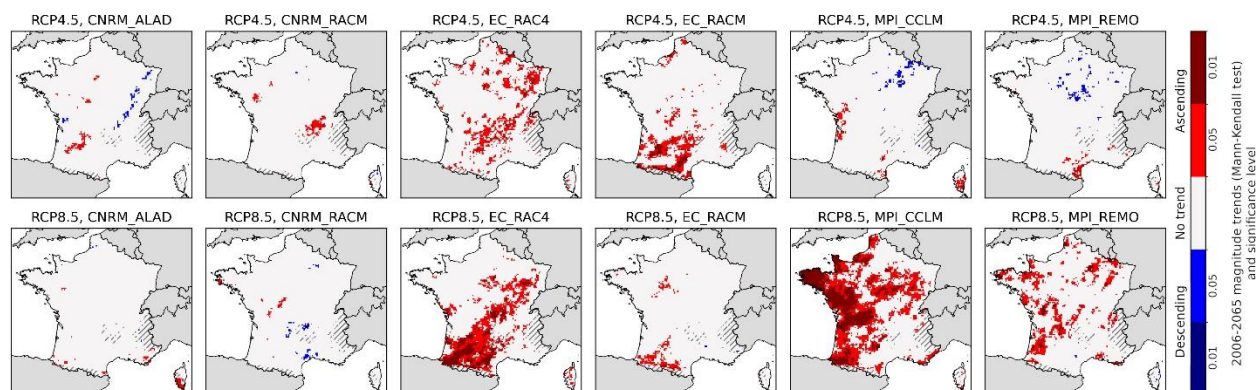
Figure 4: Results of the Mann-Kendall trend test applied to YDMI values from the 12 projected simulations, over the period 2006-2065. The ascending trends are marked with red color, while the descending trends are marked with blue color. The darker, the higher (smaller) the statistical significance (p-value). The two rows correspond to the two RCPs, and the six columns to the six models. Areas with gray hatching correspond to filtered mountain areas (average altitude > 1100 meters).
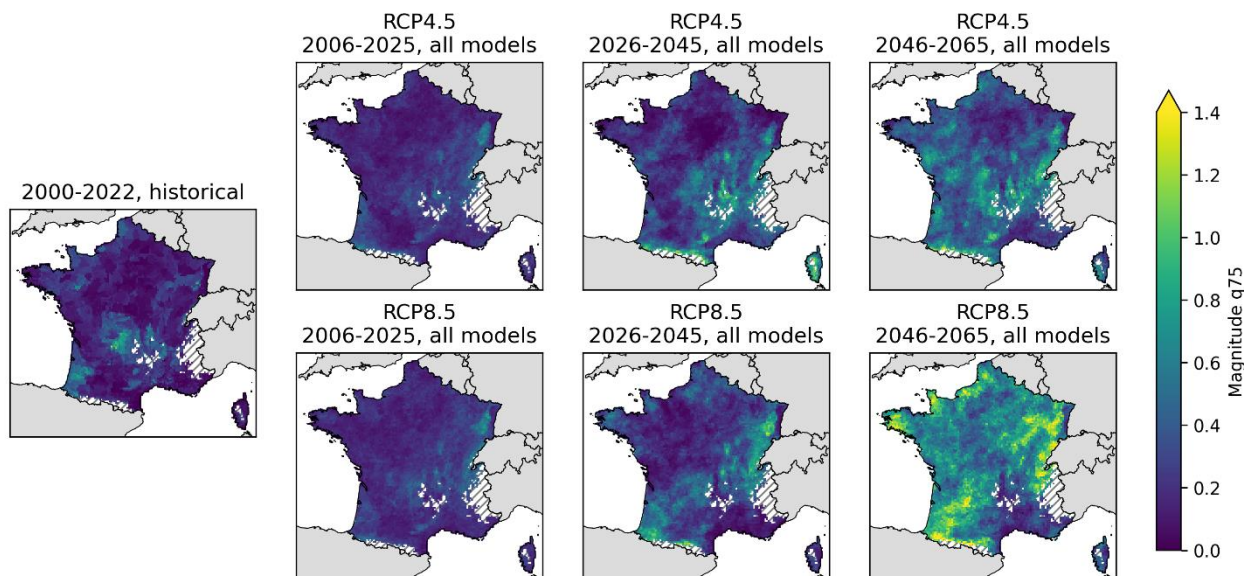
Figure 5: Third quartile (75th percentile) of YDMI, separating time horizon and RCP. Areas with gray hatching correspond to filtered mountain areas (average altitude > 1100 meters).
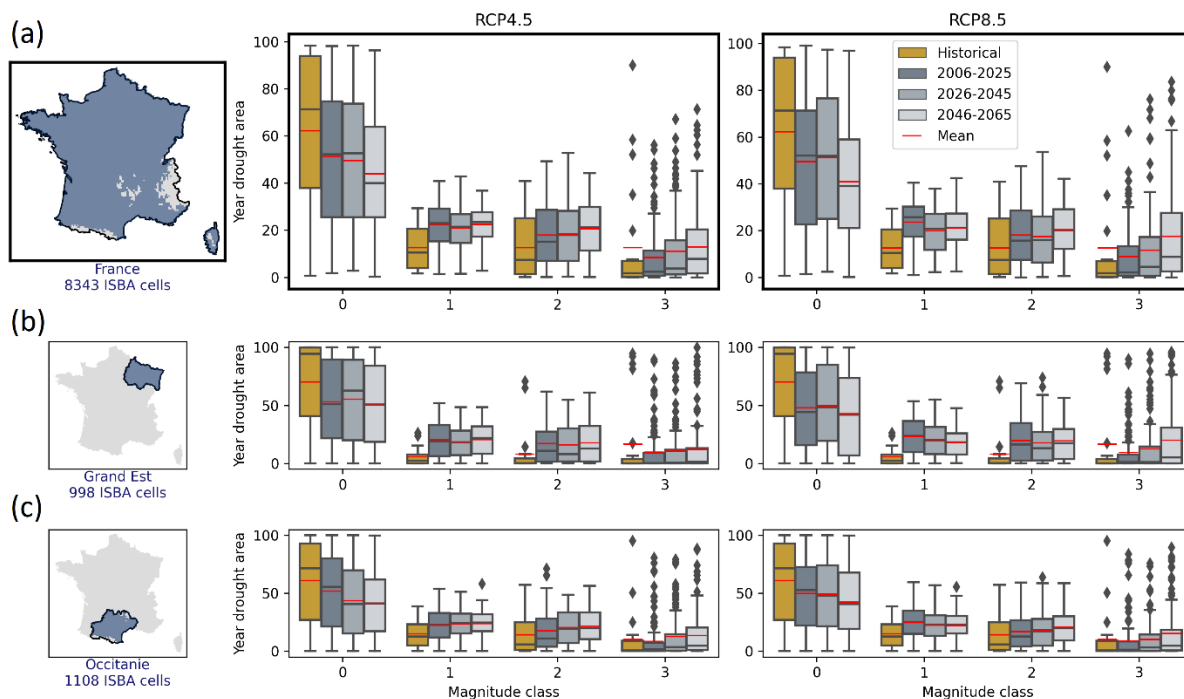
Figure 6: YDMI class fractional area expressed as % of model grid cells, separating time horizon and RCP scenario, for (a) France, (b) Grand Est region, (c) Occitanie region. Whiskers extend either to the maximum or to 1.5 * the interquartile range, equal to the difference between 75% and 25% percentiles, if inferior to the maximum. Means and outliers are shown as red features and black diamonds, respectively
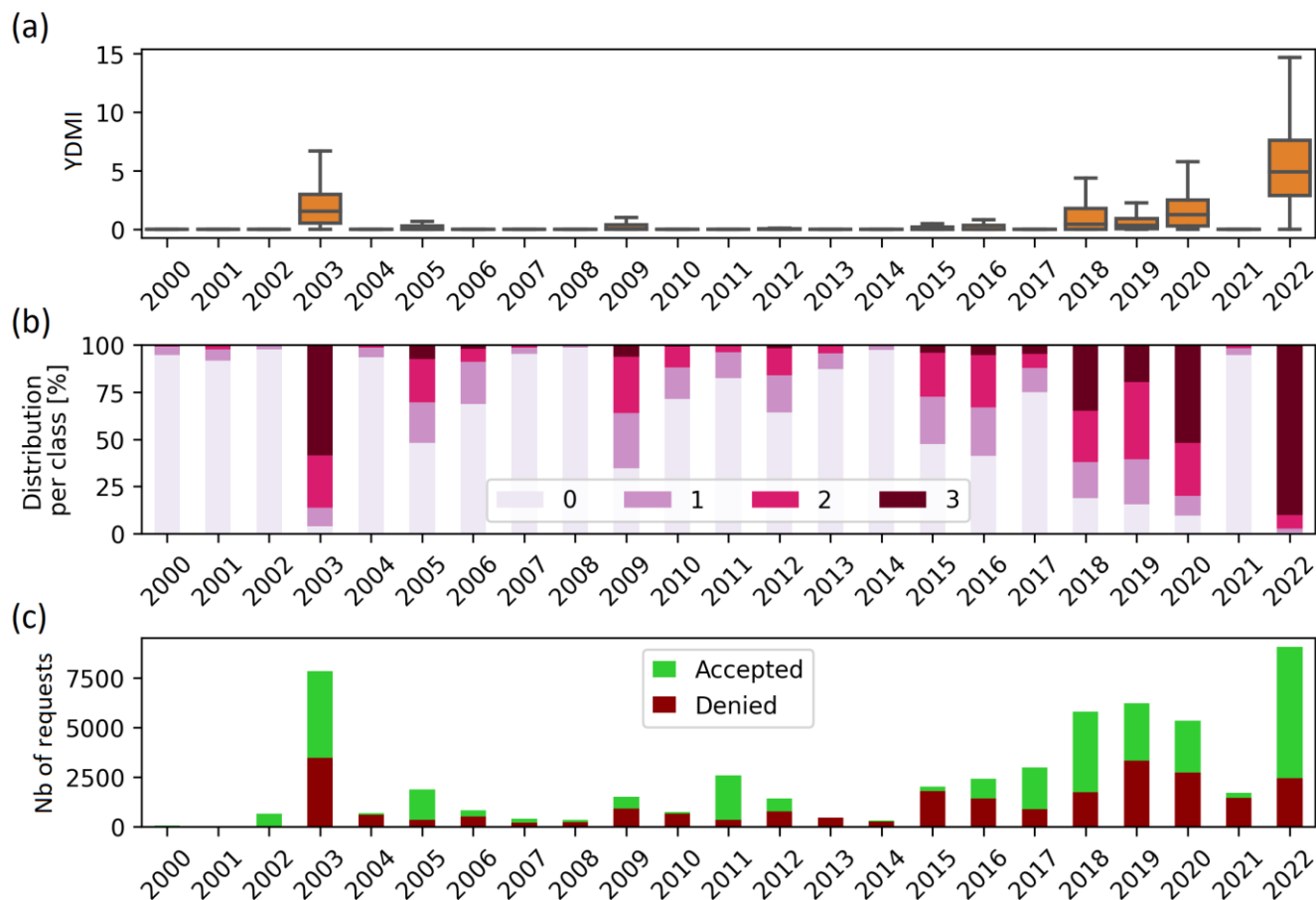
Figure 7: Year by year (a) statistical distribution of YDMI values, (b) fraction of YDMI classes (from 0 to 3), and (c) number of NatCat recognition requests, for France from 2000 to 2022. In (a), box edges and center correspond to 25%, 75% and 50% percentiles. Whiskers extend to 1.5 times the interquartile range, equal to the difference between 75% and 25% percentiles. Outliers are not displayed.